Research Article

Journal of Environmental Nanotechnology

Chavibetol Loaded Zinc Oxide Nanoparticles (CB-ZnONPs) for Activity-Enhanced Anticancer Applications against Human Lung (A549)

Balaji Murugesan, Rajesh Pattulingam* and Syed Illiyas Syed Maqbool
PG and Research Department of Chemistry, Government Arts College, Coimbatore, TN, India
Received: 21.09.2024 Accepted: 14.12.2024 Published: 30.12.2024
*gacchemistryrajesh@gmail.com

ABSTRACT

Chavibetol loaded Zinc oxide nanoparticles have demonstrated exceptional potential as anticancer agents when used together. Collectively, it possesses the capacity to serve as a substitute or addition to conventional anticancer medications. The current study focuses on examining the deliberate synthesis of biocompatible Zinc oxide nanoparticles (CB-ZnO-NPs) that are infused with chavibetol. We also assessed these nanoparticles for their ability to load and release chavibetol as a prodrug. Furthermore, the loaded particles were assessed for their ability to inhibit cell growth and induce programmed cell death in Human Lung (A549). The structure and morphological properties of the produced materials were analyzed by scanning electron microscopy, Fourier transform infrared spectroscopy, X-ray diffraction analysis, dynamic light scattering analysis, and zeta potential analysis. Dynamic light scattering (DLS) and scanning electron microscopy (SEM) examination verifies that the synthesized CB-ZnONPs have a size of around 50-60 nm. Furthermore, the analysis confirms that the nanoparticles possess a highly crystalline structure and exhibit a rod shape. The FTIR measurement confirms the conjugation of chavibetol molecules with zinc oxide nanoparticles. The X-ray diffraction patterns reveal that the zinc oxide nanoparticles possess a spinel structure and exhibit a high level of purity. Chavibetol-loaded nanoparticles exhibit a regulated release pattern in accordance with different pH levels. We observed a notable suppression of cell growth in the group that received treatment, followed by the occurrence of programmed cell death as indicated by the study of fluorescence microscopy using AO/EtBr. The Synthesized material also showed that upregulation of apoptotic protein and down regulating the antiapoptotic protein. The results of our study clearly show that chavibetol loaded zinc oxide nanoparticles may effectively transport the desired medication and induce programmed cell death in specific human lung cancer cells. This has the potential to initiate a new field in polymer surface chemistry, focusing on the creation of drug delivery systems for cancer therapies using metal oxide materials.

Keywords: Zinc oxide nanoparticles; Chavibetol; Human lung cancer; Drug release; Protein expression; Apoptosis.

1. INTRODUCTION

According to a report by the World Health Organization (WHO), cancer was responsible for 10 million deaths in 2020, making it a leading cause of death and a major obstacle to increasing life expectancy. By 2040, it is estimated that there will be around 29.5 million new instances of cancer diagnosed annually, with an expected 16.4 million deaths attributable to cancer each year. Despite the implementation of innovative medical treatments and technological developments, cancer continues to be one of the most deadly diseases (Shah *et al.* 2019). It is a pathological condition defined by the proliferation of cells beyond normal control. Cancer cells typically reside within the body and perform similar functions to normal cells. Cancer occurs when unregulated cellular replication results in abnormal and excessive growth of cells. Cancer cells possess the capacity to develop their own vascular network, detach from the primary organ, move and disseminate to other organs in the body. If proliferation is not controlled and allowed to continue and spread, it can be deadly (Kulothungan *et al.* 2022).

This is mostly because cancer cells have the ability to disregard signals, while normal cells only multiply in response to signals. It could also be attributed to genetic variations that provide control points for cell growth. Cancer can also be caused by genomic instability, which refers to an increased occurrence of changes in the genome during the whole life cycle of dividing cells. Angiogenesis is another process by which cancer advances, resulting in the formation of new blood vessels to provide metastatic cancer cells with the necessary nutrition and oxygen (Tran *et al.* 2021). Cancer does not arise from a singular causative element. The initiation of cancer is influenced by a multitude of internal and environmental variables. Internal variables encompass genetic abnormalities, genetic diseases, and hormone imbalances, whereas external causes encompass exposure to radiation, starvation, infectious agents, and tobacco use. Metastasis, often known as

tumor dissemination, is responsible for approximately 90% of cancer-related fatalities (Pang *et al.* 2006; Nishida *et al.* 2006).

In recent years, scientists have become interested in nanoparticles (NPs) because of their notable effectiveness and safety. In recent years, nanotechnology-based therapeutic and diagnostic approaches have demonstrated significant potential in enhancing cancer therapy. Nanomedicine technologies have facilitated the development of innovative cancer treatments by enabling the encapsulation of therapeutic chemicals in nanoparticulate materials and their targeted delivery to tumors through passive permeation and active internalization mechanisms. The utilization of nanoparticles for therapeutic applications has been discovered to effectively reduce resistance, hence tackling a major challenge in traditional therapy. Ongoing research is being performed to discover more accurate nanotechnology-driven cancer therapies that exhibit less detrimental effects compared to traditional treatments (Baranwal *et al.* 2023). The advancement of nanomedicine technology has led to the availability of several cancer treatment nanomedicines in the market. Additionally, numerous nanomedicines employing different nanosystems such as metallic nanoparticles, liposomes, quantum dots, carbon nanotubes, polymeric micelles, and nanospheres are currently in advanced stages of development and clinical testing (Alrushaid *et al.* 2023). Zinc oxide nanoparticles (ZnO-NPs) are extensively used in medication delivery, cancer diagnostics, and treatment because of their distinct physical and chemical characteristics. ZnO-NPs have demonstrated efficacy not just in combating cancer but also in addressing numerous other ailments across various sectors like cosmetics, electronics, and the textile industry. ZnO-NPs can be generated using chemical, physical, or biological methods. Precipitation, microemulsion, chemical reduction, sol-gel, and hydrothermal techniques are among the chemical methods that necessitate significant energy consumption and the maintenance of high pressure or temperature during the synthesis process (Anjum *et al.* 2021). ZnO-NPs can be produced via physical techniques such as vapor deposition, plasma, and ultrasonic irradiation, which are less frequently used compared to chemical procedures. However, these methods generally need a significant amount of energy and large machinery, resulting in increased costs for the items. Biological synthesis is an alternative approach for producing ZnO-NPs that is considered to be more environmentally friendly. Regardless of the approach used, all forms of ZnO nanoparticles have demonstrated effectiveness in addressing cancer through their ability to diagnose, treat, and deliver anticancer medications in a sustained and focused manner (Aljabali *et al.* 2022). Zinc oxide nanoparticles (ZnO-NPs) are extensively utilized in various industries and research organizations due to their large range of applications. Due to the minute particle size of nano-ZnO, zinc can be readily absorbed by the human body. Due to its cost-effectiveness and lower toxicity compared to other metal oxide nanoparticles, ZnO-NPs have diverse applications in medicine, such as antibacterial, anti-diabetic, anti-inflammatory, anti-aging, wound healing, and bio-imaging (Jin *et al.* 2019).

ZnO-NPs exhibit excellent biocompatibility, making them suitable for therapeutic applications due to their antibacterial, antifungal, antiviral, and anticancer characteristics. Various inorganic metal oxides, including TiO_2, CuO, and ZnO, have been synthesized and are currently being studied. Among these metal oxides, ZnO-NPs are particularly intriguing because of their affordability, safety, and ease of preparation. Moreover, any agent designed for human ingestion for the purpose of treating specific disorders must possess the following properties. The substance should be non-toxic, inert towards food and the container, possess a nice taste or be devoid of taste, and not emit an unpleasant odor (Asif *et al.* 2023). ZnO-NPs are an example of an inorganic metal oxide that fulfills all the specified requirements, making them suitable for usage as a medicine, package preservative, and antibacterial agent without any safety concerns. Therefore, the US Food and Drug Administration (FDA) has categorized ZnO-NPs as a "GRAS" (generally regarded as safe) chemical. ZnO-NPs possess a significant band gap of 3.37 eV and a high exciton binding energy of 60 meV. As a result, they exhibit a diverse spectrum of semiconducting properties, such as robust catalytic activity, optical characteristics, UV filtering capabilities, anti-inflammatory effects, and wound healing properties. Additionally, they have been extensively utilized in cosmetic products, such as sunscreen creams, owing to their exceptional UV filtering properties. ZnO-NPs were initially employed in the rubber sector to enhance the durability of rubber composites, strengthen high polymers, and provide anti-aging characteristics. ZnO-NPs have garnered interest in the field of biological imaging because of their capacity to display luminescence. In addition, they have also garnered the attention of researchers who are interested in developing diagnostic tools, as they can also be utilized in biosensing applications (Siddiqi *et al.* 2018).

Chavibetol is an organic substance belonging to the phenylpropanoid class. It is a major component of the essential oil derived from the leaves of the betel plant (*Piper betel*) and catania (Aara *et al.* 2020). This substance is a fragrant chemical that emits a pungent scent. Zinc oxide (ZnO) is used in contemporary drug delivery systems because of its convenient production, affordable price, adaptable structure, lack of toxicity, substantial drug-carrying capacity, programmable drug release capability, and ability to deliver drugs to specific targets. Porous ZnO structures, including porous nanotubes, porous nanobelts, porous nanorods, and porous cages, have been effectively employed in targeted drug delivery systems. To ensure efficient medication

delivery, the surface of nanoparticles can be modified through the use of different agents such as ligands, linker chains, medicines, and markers. Nanoparticles (NPs) aggregate in cells by engaging in certain molecular interactions, such as receptor-ligand interactions. Upon receiving a suitable stimulus, the nanoparticles undergo endo/lysosomal escape and release the drug, leading to the destruction of its intended target. Different forms of internal and exterior stimuli are also involved in the precise administration of anticancer medications (Martínez *et al.* 2018).

The objective of this study was to create zinc oxide nanoparticles using a hydrothermal approach, while being able to adjust the parameters and improve their biocompatibility. In addition, their typical drug encapsulation and release capabilities were assessed, taking into account their response to different pH levels in the system. Furthermore, chavibetol loaded zinc oxide nanoparticles were created and analyzed to investigate their potential as anticancer agents in lung cancer cells.

2. MATERIALS AND METHODS

Zinc nitrate $Zn(NO_3)_2$ and sodium hydroxide (NaOH), methanol (CH_3OH) and ethanol (C_2H_5OH) were purchased from Merck Life Science Pvt. Ltd. Mumbai, India. Chavibetol was purchased from Sigma Aldrich Bengaluru, India. Cell culture media, MTT [3-(4,5-dimethyl-2-thiazolyl) 2,5 diphenyl-2-H-tetrazoliumbromide] and Dulbecco's modified eagle medium-high glucose (DMEM-HG) were acquired by Hi-Media Laboratories Pvt. Ltd, Mumbai, India. Acetone, DMSO, ascorbic acid and DPPH (2,2-diphenyl-1-picryl-hydrazyl) were acquired from Thomas Baker India. The cell line used in this study was acquired from the National Centre for Cell Science (NCCS), Pune, India. All chemicals were used in their original form. Double distilled water was used in all experiments.

2.1 Synthesis of ZnO Nanoparticles

ZnO nanoparticles were synthesized by hydrothermal technique. Zinc nitrate (0.1 M) and methanol (50 ml) were mixed in a beaker under continuous stirring at room temperature for 60 min. Subsequently, 0.4 M NaOH solutions (25 ml) were added in a dropwise manner with continuous stirring of the solution. The mixture was then heated at 180 °C for 12h in an autoclave made of stainless steel and possess Teflon chamber. The solution was then allowed to cool at room temperature. The precipitate was formed inside the Teflon chamber. The precipitate was then filtered and washed several times with distilled water and absolute methanol. The final product was dried in an oven at 60◦C.

2.2 Synthesis of CB-ZnO Nanoparticles

Chavibetol loaded ZnO nanoparticles (CB-ZnO-NPs) were synthesized as per previously reported method with minor modification. Briefly, 500 mg chavibetol was dissolved in 50 ml 0.001 N NaOH solution and the required amount (100 mg) of ZnO nanoparticle was added into the chavibetol solution with constant stirring for 60 min at 80 °C to obtain the homogeneous mixture. Later, this homogeneous mixture was sonicated for 180 min to form the chavibetol loaded ZnO nanoparticles. The obtained nanoparticles (CB-ZnO-NPs) were centrifuged and washed using ethanol and dried in the oven at 60 °C.

2.3 FT-IR Characterization

Fourier transforms infrared (FT-IR) spectroscopy of CB-ZnO-NPs were performed by using Nicolet 5700 instrument (Nicolet Instrument, Thermo Company, USA) with KBr pellet method. Each KBr disk was scanned over a wave number region of 500-4000 cm^{-1}.

2.4 X-Ray Diffraction Analysis

The method of X-ray diffraction (XRD) was used to investigate the crystalline structure of CB-ZnO-NPs. The scanning rate employed was $1^{o}min{-}1$ over the 10–80° 2θ range.

2.5 Zeta Potential Analysis

The zeta potential of the synthesized nanoparticles was determined by means of a zeta potential analyzer (90 Plus Particle Size Analyzer, Brookhaven Instruments Corporation, using Zeta Plus software). The measurement of zeta potential is based on the direction and velocity of particles under the influence of a known electric field.

2.6 Particle Size Analysis

The particle size range of the CB-ZnONPs along with its polydispersity was determined using a particle size analyzer (90 Plus Particle Size Analyzer, Brookhaven Instruments Corporation). Particle size was arrived based on measuring the time dependent fluctuation of scattering of laser light by the nanoparticles undergoing Brownian motion.

2.7 Scanning Electron Microscope (SEM) Analysis

The samples were placed on polycarbonate substrate and the excess water was left to dry at room temperature (JSM5600LV, JEOL, Japan) operating at an accelerating voltage of 20 kV.

2.8 Chavibetol Loading and Encapsulation Efficiency

Chavibetol 3mg loaded ZnO nanoparticles were dispersed into 6ml of phosphate buffer solution (PBS) and centrifuged at 12,000 rpm for 30 min. The supernatant was collected to measure the ultraviolet absorption at 280nm. The loading efficiency and encapsulation efficiency of Chavibetol loaded ZnO nanoparticles were calculated as follows.

$$\text{Loading Efficiency} = W_0 / W \times 100\%$$

$$\text{Encapsulation Efficiency} = W_0/W_1 \times 100\%$$

Where, W_0 is the amount of Chavibetol enveloped in the ZnO nanoparticles, W is the amount of ZnO-NPs nanoparticles, and W_1 is the amount of Chavibetol added in the system.

2.9 In Vitro Drug Release Study

The chavibetol loaded nanoparticles were transferred to a beaker containing 100mL of phosphate buffer (pH 5.5, 6.8 and 7.4) with continuous stirring at 100 rpm. The sink condition was maintained by periodically removing a 2ml sample and replacing an equal volume of buffer. The amount of chavibetol release was analyzed with a spectrophotometer at 485 nm. The experiments were performed in triplicate for each of the samples.

2.10 Cell Viability Assay

Cell viability was determined by measuring the ability of cells to transform MTT to a purple formazan dye. Cells were seeded in 96-well tissue culture plates at $2x10^3$ cells per well for 24 hours. The cells were then incubated with chavibetol, loaded and unloaded nanoparticles at different concentrations for different time periods. After treatment, 200 ml of MTT solution was added per well and incubated for another 5h. To dissolve the formazan salt formed, the medium was aspirated and replaced with 150 ml of DMSO per well. The cell growth conditions were recorded by the color intensity of the formazan solution. Absorbance at 570nm was recorded on a 96 well microplate reader.

2.11 Morphological Study

The human lung cancer cells (A549) that were grown on coverslips ($1x10^5$ cells per coverslip) were incubated for 6-24 h with compounds at the IC_{50} concentration, and they were then fixed in ethanol: acetic acid solution (3:1; v/v). The coverslips were gently mounted on glass slides for morphometric analysis. Three monolayers per experimental group were photomicrographed. The morphological changes of the selected cancer cells were analyzed using a Nikon (Japan) bright field inverted light microscope at 20 x magnifications.

2.12 Fluorescence Microscopic Analysis of Cell Death

Approximately 1 ml of a dye mixture, 100 mg ml acridine orange (AO) and 100 mg ml ethidium bromide (EtBr) in distilled water was mixed with 9 ml of cell suspension ($1x10^4$cells per ml) on clean microscope coverslips. The cells were collected, washed with phosphate buffered saline (PBS) (pH 7.2) and stained with 1 ml of AO/EtBr. After incubation for 2 min, the cells were washed twice with PBS (5 min each) and visualized under a Fluorescence microscope (Nikon Eclipse, Inc, Japan) at 20x magnification with an excitation Filter at 480 nm. The same procedure was also followed for DAPI.

2.13 Protein Expression Analysis

The impact of CB-ZnONPs on apoptotic and anti-apoptotic proteins in both treated and untreated cells was determined by Western blotting. The selected PB-ZnONPs incubated the cells for 24 hours in a 100 millimeter culture dish. The media was subsequently extracted, and the analysis was conducted.

3. RESULTS AND DISCUSSIONS

For this investigation, we utilized chavibetol as the medication of interest for targeted delivery into human cancer cells. Figure 1 depicts the chemical composition of chavibetol. Prior research has indicated that chavibetol has a significant role in the proliferation of cancer cells. The overall functional efficacy of nanoparticle-based delivery systems is mostly determined by the physicochemical characteristics of the nanoparticles, including their size, shape, and physical state.

3.1 Encapsulation Efficiency

The chavibetol loading and encapsulation efficiency of zinc nanoparticles with different chavibetol concentrations was found to be proportional to the chavibetol concentration. The nanoparticles with 40mg/ml of chavibetol showed highest encapsulation efficiency 88.6% respectively. The percentage of ZnO-NPs entrapped in the chitosan shell relative to the initial encapsulation amount was called particle entrapment efficiency. The ZnO-NPs biosynthetic plant extract entrapment efficiency was measured. The ZnO-NPs from 0, 1, 5, 10, 15, and 20 mL of Plumeria extract had 65%, 73%, 77%, 80%, 82%, and 82% efficiencies. Encapsulated ZnO-NPs from 15 mL plant extract have the maximum entrapment effectiveness of 82%. Encapsulated ZnO-NPs without plant extract have the lowest entrapment efficiency of 65%. Entrapment

efficiency rises with plant extract, reaching a constant value of 82% at 15 mL. The DEE increases with plant extract concentration because biological compounds like plant alkaloids encapsulated on ZnO-NPs may have improved the interaction between ZnO nano-surface and chitosan molecules (Halanayake *et al.* 2021).

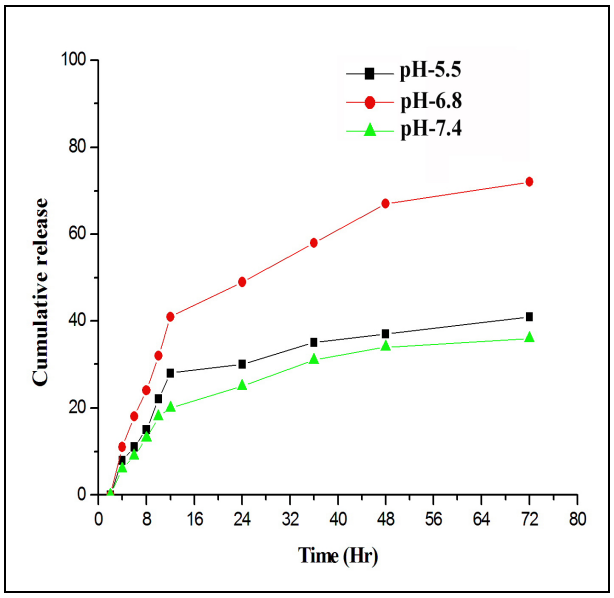

Fig. 1: Drug release study of CB-ZnO-NPs

3.2 Drug Release Study

The ability of the carrier to release the goods efficiently at the desired site is an important feature of any delivery system. (Fig. 1) depicts the release of chavibetol from the Zinc oxide nanoparticles in phosphate buffer (pH 7.4). At the end of 72 hours incubation, 74% of chavibetol was released in phosphate buffer. This revealed that the release of chavibetol was higher in acidic pH. This pH dependent release may help to improve the efficacy of chavibetol release into the system. This may initiate rapid release of chavibetol from the nanoparticles after internalization in the system. Such efficient release would ultimately result in improved anticancer activity against lung cancer system. It is evident that the medication is not released uniformly over the initial 7 hours at acidic pH values. At a pH of 5.0, there is a reported release of zinc oxide nanoparticles that fluctuates both negatively and positively. This fluctuation may be attributed to variations in the porosity of the manufactured nanoparticles. It is noted that particles with higher porosity contain more cisplatin, resulting in an overall uniform release. However, at pH levels of 6.0 and 4.0, we see a nearly consistent release of cisplatin, except for a brief period of 5-6 hours at pH 6.0. At these specific pH values, the particles exhibit increased stability, resulting in the occurrence of only diffusion. This phenomenon accounts for the exceptionally gradual release of the encapsulated cisplatin concentration (Abayarathne *et al.* 2020).

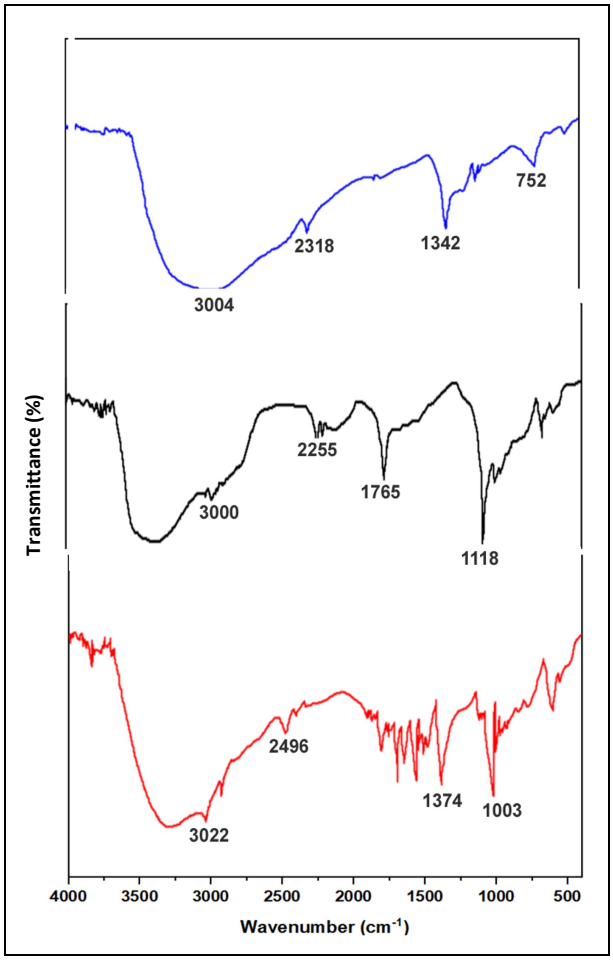

Fig. 2: FTIR spectra of a) Zinc oxide NPs; b) Chavibetol; c)CB-ZnO-NPs

3.3 FTIR

The functional characteristics of ZnO-NPs, chavibetol and CB-ZnO-NPs were investigated by using FTIR technique. The FTIR spectra (Fig. 2) exhibited a broad peak at 3004 cm-^{1}, 2318 cm-^{1} due to the –OH stretching of the hydroxyl group, which arose due to the hygroscopic properties of ZnO-NPs. Small peaks between 752 cm^{-1} were due to -CH stretching mode of alkane groups. The most prominent characteristic peaks at 2255 and 1765 were observed due to carboxylate asymmetrical and symmetrical stretching in the chavibetol (Fig. 2b). Carbon probably comes from methanol. The main peak was observed at 2496 cm^{-1} and 1374 (Fig. 2c) due to metal-oxygen (Zn-O) stretching. The primary distinguishing peaks observed in the betel leaf extract are located at 1030, 1532, 1635, 2360, 2920, and 3220 cm^{-1}, as illustrated in Fig. 2. The peak observed at 1635 cm^{-1} is indicative of C–O stretching vibrations commonly found in ketones, aldehydes, and carboxylic acids. Alternatively, it may be attributed to the deformation of the amine group, most likely originating from indole-3-acetic acid. The transmittance peaks at 1025, 1532, 2360, 2920, and 3220 cm^{-1} are indicative of

certain molecular vibrations. These peaks correspond to the stretching of C–O–C bonds, the stretching of N–H bonds (indicating the presence of primary amine), the stretching of C–H bonds, and the stretching of –OH/N–H bonds, respectively. The composite film (PVA-Betel) exhibits all the prominent absorption peaks of PVA (3294, 2920, and 1090 cm^{-1}) and betel leaf extract (2360 cm^{-1}) with a small alteration in position or broadening of the peaks. The shift of the peak from 2360 cm^{-1} to 2358 cm^{-1} indicates the establishment of hydrogen bonds between the amine groups in betel leaf and the –OH groups in the PVA composite film (Li *et al.* 2015).

3.4 XRD

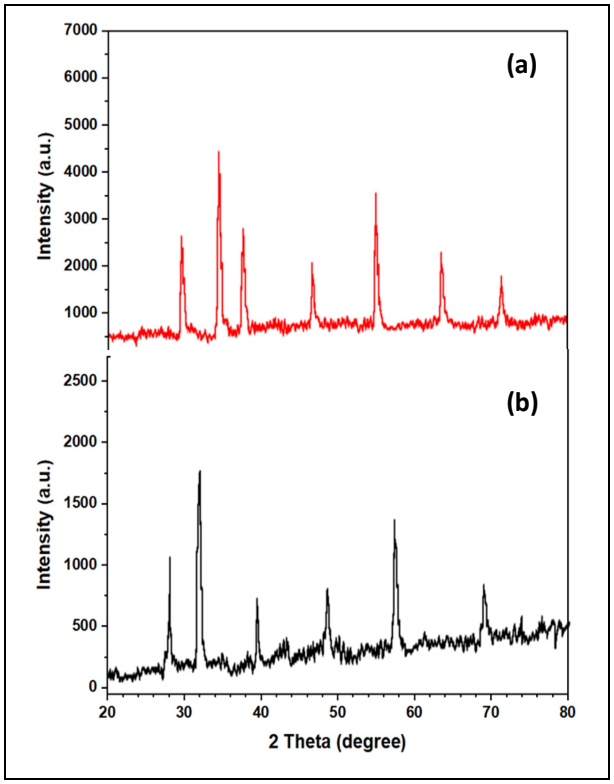

Fig. 3: XRD pattern of ZnONPs and CB-ZnO-NPs

The crystallinity of CB-ZnO-NPs was investigated by using XRD technique as illustrated in Fig. The XRD spectra of CB-ZnO-NPs (Fig.3) exhibited several characteristic peaks at 2θ=31.86, 34.31, 36.00 47.62, 56.74, 63.01, 68.20, 72.50 and 77.04, assigned to (100), (002), (101), (102), (110) (103) (112) (004) and (211) of ZnO nanoparticles; these results indicate that the structure of ZnO nanoparticle is polycrystalline in nature (JCPDS 50664). The XRD pattern of ZnONPs exhibited a broad peak at 2θ = 24.35° and some additional peaks of ZnO-NPs were also visible, confirming the presence of zinc as shown in Fig. 3a. The phase crystalline nature and purity of the generated ZnO powder sample were analyzed using XRD analysis. The X-ray diffraction (XRD) patterns of zinc oxide nanoparticles (ZnO-NPs) are presented in Fig. 3. The sample exhibited prominent and well-defined diffraction peaks, indicating a high degree of crystallization of the ZnO-NPs. The X-ray diffraction (XRD) spectra confirmed the presence of the hexagonal (wurtzite) phase of crystalline ZnO, with a space group of lattice constants of a = 3.253 (Å) and c = 5.213 (Å). After loading with chavibetol the crystalline nature of particles still remains in such conditions (Fig. 3b). The XRD analysis did not detect any additional crystalline phases associated with contaminants, indicating that the synthesized ZnO-NPs have a high purity of the wurtzite phase. Moreover, the highest level of intensity observed in the ZnO-NPs sample occurred at an angle of 2θ = 36.275°, which corresponds to the (101) lattice associated with the wurtzite ZnO phase (Saddik *et al.* 2022).

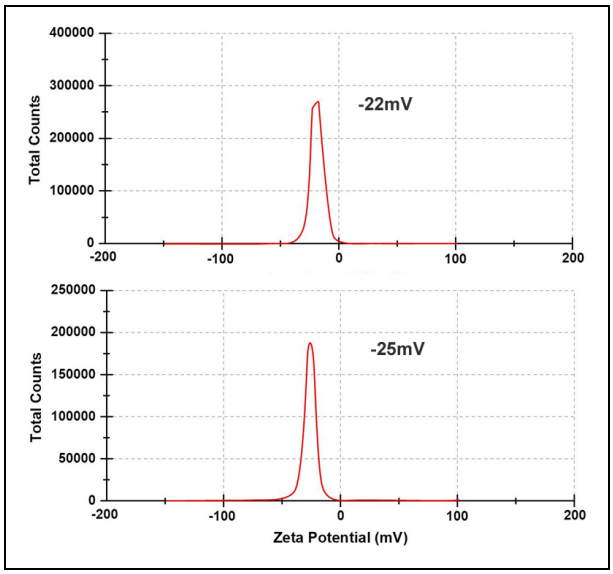

Fig. 4: Zeta potential distribution of ZnONPs and CB-ZnO-NPs

3.5 Zeta Potential and Particle Size Analysis

The Zeta potential of ZnO-NPs nanoparticle, chavibetol and CB-ZnO-NPs and were evaluated by measurement of zeta potential. The zeta potential of ZnO nanoparticle, chavibetol and CB-ZnO-NPs was -25mV respectively as shown in Fig. 4a, whereas the unloaded ZnO was 22mV (Fig. 4b) indicating that chavibetol loaded ZnO nanoparticles were more stable as compared to ZnO nanoparticle due to the high charge repulsion between the nanoparticle (-30 mV charge is a sufficient charge to prevent accumulation and dispersed particle adhesion). The zeta potential conductivity and stability of ZnO-NPs were increased after the coating of chavibetol onto ZnONPs which was appropriate for the drug delivery application. The particle size of CB-ZnONPs was also investigated. The particle size of CB-ZnO-NPs was found to be in the range of 46.5 nm to 70 nm. DHA has the potential to enhance the dimensions of ZnO nanoparticles. However, the measured zeta potential for DHA-loaded ZnO-NPs dispersed in distilled water was

approximately -35 mV. This indicates that the incorporation of DHA inside ZnO-NPs and the physical stability of the resulting nanocomposite are both favorable.

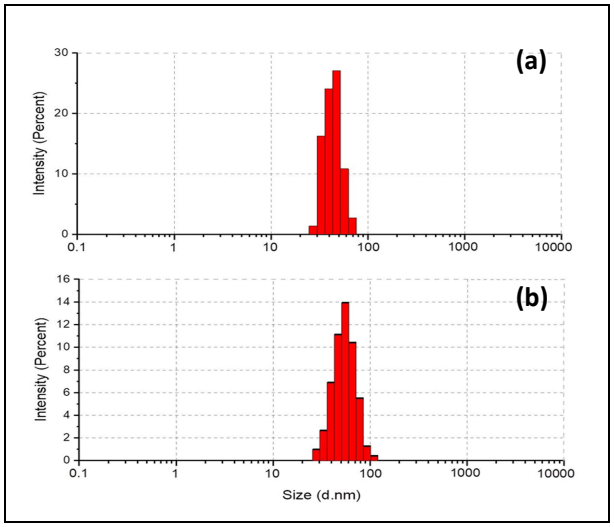

Fig. 5: DLS analyzer of ZnONPs and CB-ZnO-NPs

3.7 SEM

The surface morphology of the powder was analyzed using a scanning electron microscope. The rod-shaped nanoparticle exhibited porous characteristics and achieved a length of 50-60 nm. The morphologies of each sample exhibited substantial dissimilarities in this instance. For this particular study, a rod with a modest porous structure is typically favored. Prior research has demonstrated that ZnO in the form of rod structures exhibits superior optical characteristics. The ZnO crystals obtained from isopropanol exhibit a distinct morphology of elongated rods with a hexagonal cross-section. In contrast, the crystals obtained from ethanol have a less defined crystalline structure and seem disc-like with a hexagonal cross-section (Vimala *et al.* 2014).

3.8 MTT Assay

We analyzed the effect of the CB-ZnO-NPs on the cell response of the Human lung cancer cells by using the MTT assay. Fig 7 (A549) shows the *in vitro* cytotoxicity activity of extract (up to 100µg/ml concentrations) against selected cancer cells. The experimental results demonstrate that the CB-ZnO-NPs inhibited cell proliferation in a dose dependent manner.

3.6 DLS

The DLS apparatus is capable of quantifying the thickness of a protective or stabilizing layer surrounding metallic particles, as well as determining the size of the metallic core itself. The average size of the CB-ZnO-NPs was determined using DLS measurement. The mean diameter for the green production of ZnO-NPs was 50 nm (Fig. 5a), and the chavibetol loaded ZnO-NPs was 50 nm (Fig. 5b). The observed high particle size in DLS is attributed to the inclusion of bio-organic molecules surrounding the core of the Au NPs in the measured size. Additionally, the significant particle size may also result from the many forces of interaction in the solution, such as van der Waals interactions. The variations in particle sizes acquired using microscopic techniques were attributed to disparities in sample preparation and the polydispersity of the sample, as measured by DLS.

Various methodologies yield varying average sizes, contingent upon the instrument's sensitivity to factors such as particle count, volume, mass, or optical characteristics. However, this is typically not true for bio-based synthesis processes that generate polydisperse particles. Hence, it is crucial to exercise a high level of prudence when measuring particle sizes using different methods in a bio-based procedure and when comparing them to ascertain their reactivity for certain purposes.

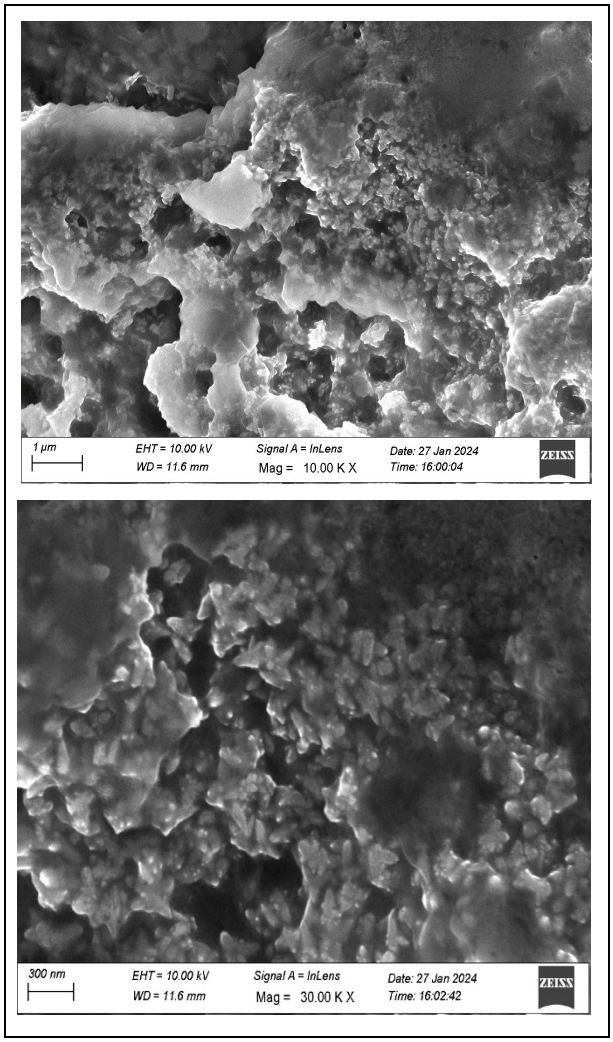

Fig. 6: SEM images of CB-ZnO-NPs

From Fig. 7 the IC_{50} values of ZnO-NPs, Chavibetol, CB-ZnO-NPs against cancer cells were calculated and it is found to be 25, 21µg/ml and 9µg/ml respectively. The observed IC_{50} values results that drug loaded ZnO-NPs are comparably significant and inhibits the proliferation of selected Human Lung cancer cells. Cell viabilities were assessed at three distinct concentrations (0.6 µg/mL, 0.7 µg/mL, and 0.8 µg/mL) of free DOX, blank zinc oxide nanoparticles, a combination of DOX and blank nanoparticles, and nanoparticles loaded with the drug. The study's findings unequivocally demonstrate that ZnO nanoparticles possess inherent cytotoxicity, as evidenced by a reduction in cell viability to 98%, 84%, and 77% at the corresponding concentrations. Additionally, it has been discovered that the effectiveness of the potent anticancer medicine DOX is greatly enhanced ($p < 0.05$) when zinc oxide is introduced alongside it. This can be attributed to the increased absorption of DOX in the presence of ZnO nanoparticles, which demonstrated a combined action of both cytotoxic chemicals, namely ZnO nanoparticles and DOX (Vimala *et al.* 2014).

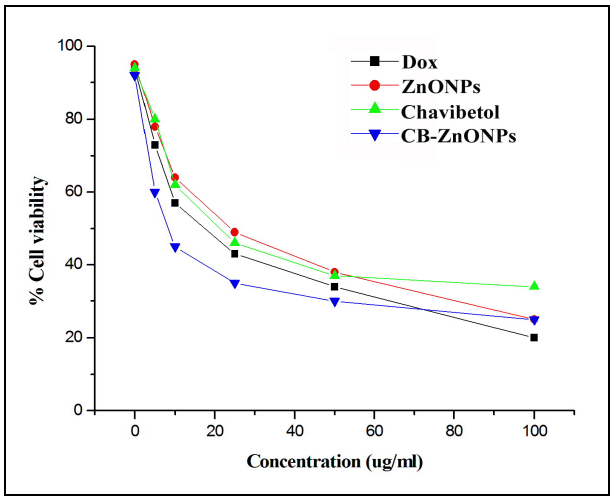

Fig. 7: Cytotoxic analysis of synthesized nanomaterials on Human Lung cancer cell (A549)

3.9 Cell Morphology Analysis

The morphological changes of selected cancer cells in the absence and presence of material at various concentrations are shown in Fig. 8-10 (A549). It could be observed that control cells did not show any remarkable changes in their morphology. However, in the presence of ZnO-NPs, Chavibetol and CB-ZnO-NPs, the cells show improved cell shrinkage, membrane blebbing and forms floating cells in a dose-dependent manner. It is well accepted that cytological investigations elucidate the antiproliferative effect routed through membrane blebbing, membrane instability and distressing of the cytoskeleton of the cells by the CB-ZnO-NPs compared to other chavibetol and ZnO-NPs alone. Based on the findings presented here, the CB-ZnO-NPs nanoparticle demonstrated inherent anticancer capabilities. Multiple studies have shown that the production of reactive oxygen species (ROS) is a crucial mechanism by which zinc nanoparticles cause cell death.

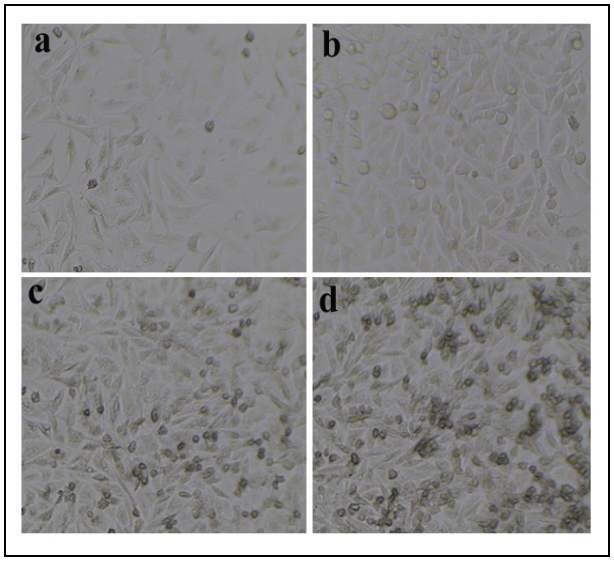

Fig. 8: Morphometric analysis of synthesized ZnO-NPs on A549 cells under phase contrast inverted microscope a) Control b) 5µg/ml, c) 10µg/ml, d) 25µg/ml of ZnO-NPs treated cells

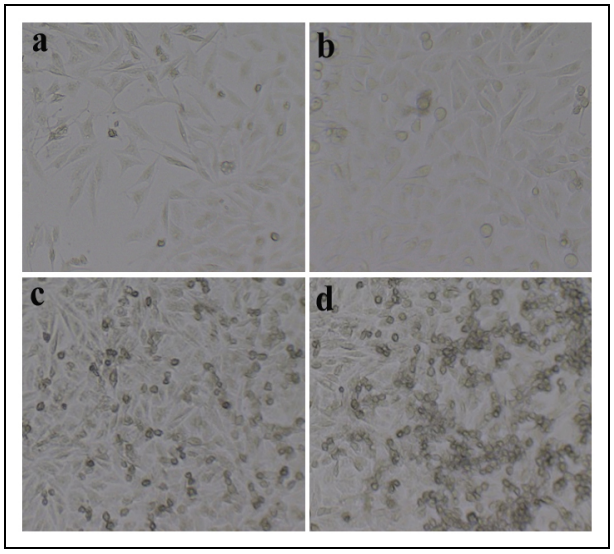

Fig. 9: Morphometric analysis of Chavibetol on A549 cells under phase contrast inverted microscope a) Control b) 5µg/ml, c) 10µg/ml, d) 25µg/ml of Chavibetol treated cells

Reactive oxygen species (ROS), including superoxide, hydroxyl radicals, and hydrogen peroxide, are continuously produced and removed in biological systems. ROS, or reactive oxygen species, are widely recognized for their significant contributions to various normal biochemical functions and abnormal disease processes. Oxidative stress occurs in cells when there is an excessive buildup of reactive oxygen species (ROS)

that surpasses the capacity of the cellular antioxidant defense system. This leads to the impairment of cellular components such as lipids, proteins, and DNA.

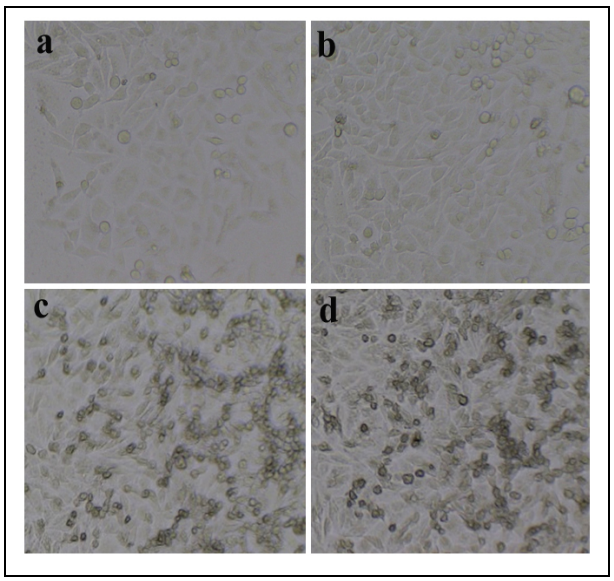

Fig. 10: Morphometric analysis of synthesized CB-ZnO-NPs on A549 cells under phase contrast inverted microscope a) Control b) 5µg/ml, c) 10µg/ml, d) 25µg/ml of CB-ZnO-NPs treated cells

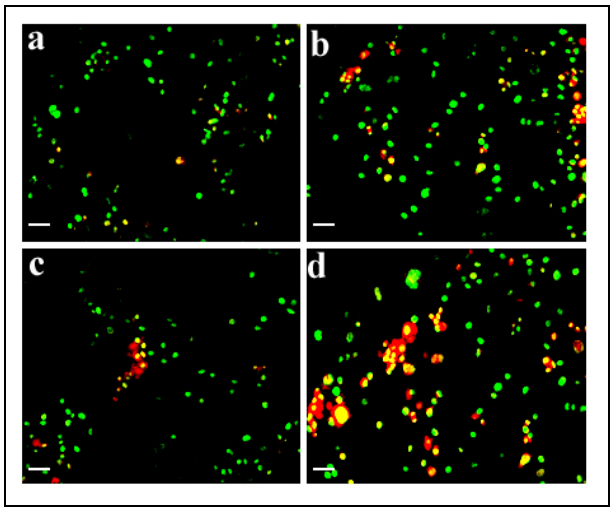

Fig. 11: AO/EtBr fluorescent analysis of synthesized ZnONPs on A549 cells under phase contrast inverted microscope a) Control b) 5µg/ml, c) 10µg/ml, d) 25µg/ml ZnONPs treated cells. The scale bar measures about 50µm

3.10 Acridine Orange /Ethidium Bromide (AO/EtBr) Staining Method

In order to study the effect of apoptogenic activity of the material on cancer cells we conceded out the fluorescence microscopic analysis. Fluorescence microscopy images of A549 cells in the absence of material. Fig 11-13 (A549), (a) shows that the untreated A549 cells (control) did not show any significant adverse effect compared to the material treated cells (Fig. 13(b to d). From the analysis, it can be observed that with the addition of ZnO-NPs, Chavibetol and CB-ZnO-NPs to the A549 cells, untreated cells not shown any significant changes nanoparticle treated cells showed bright fetches of fluorescence the condensed chromatins and nuclear fragmentation in treated cancer cells. In addition, taken all together, the apoptotic potential was significantly found in CB-ZnO-NPs, ZnO-NPs and Chavibetol orderly. The analysis of apoptotic cells challenged with CB-ZnO-NPs was conducted by double labeling with AO/EtBr, as shown in Fig.

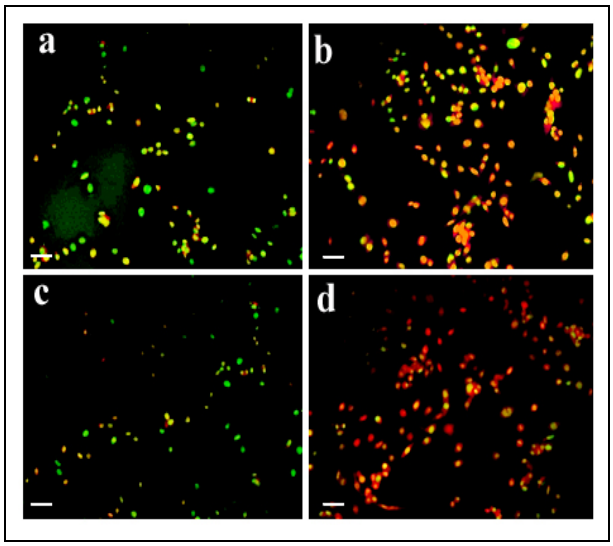

Fig. 12: AO/EtBr fluorescent analysis of synthesized chavibetol on A549 cells under phase contrast inverted microscope a) Control b) 5µg/ml, c) 10µg/ml, d) 25µg/ml chavibetol treated cells. The scale bar measures about 50µm

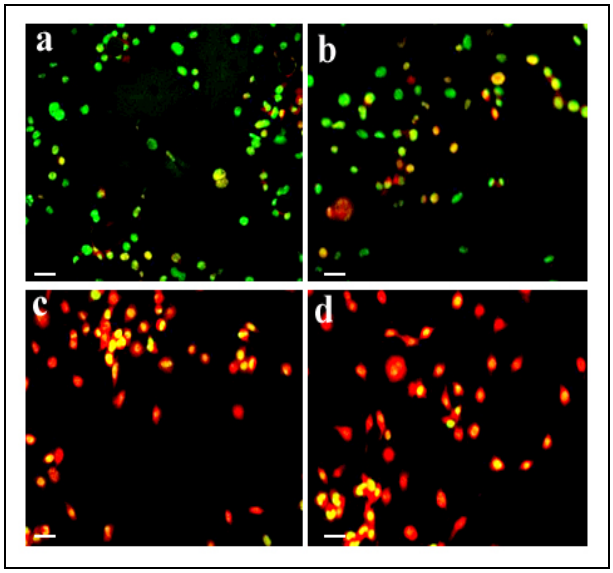

Fig. 13: AO/EtBr fluorescent analysis of synthesized CB-ZnONPs on A549 cells under phase contrast inverted microscope a) Control b) 5µg/ml, c) 10µg/ml, d) 25µg/ml chavibetol treated cells. The scale bar measures about 50µm

EtBr, a red fluorescence stain, penetrated the nuclei of apoptotic cells, while AO, a green dye, was only taken up by normal cells. The control cells exhibit a significant level of green fluorescence in the nucleus, indicating the presence of living cells. The addition of CB-ZnONPs (at concentrations of 5, 10 and 25µg/ml) to the cells resulted in an orange hue, indicating early apoptosis, and red stained fragmented nuclei, indicating delayed apoptosis. Oxidative stress mostly results in lipid peroxidation, which is produced by excessive production of free radicals. Cancer cells can experience apoptosis as a result of reactive free radical-induced lipid peroxidation (LPO) and decreased levels of natural antioxidants. HeLa cells treated with ZnO nanoparticles produced by fungi showed increased production of reactive oxygen species (ROS) and reduced antioxidant activity. This could be attributed to the excessive release of dissolved zinc ions, which stimulates the development of intracellular reactive oxygen species (ROS) in cancerous cells and triggers apoptosis through the apoptotic signaling pathway. Redox-active modification enables metals to function as pro-oxidants through Fenton and Fenton-like reactions and redox-cycling, resulting in the generation of hydroxyl free radicals. Oxidative stress generated by ROS can lead to damage in the DNA, protein, and lipids of cancer cells by controlling the expression of the p53 protein. The presence of reactive oxygen species (ROS) can trigger cellular responses through the oxidation of redox-sensitive transcription factors and intermediate signaling molecules.

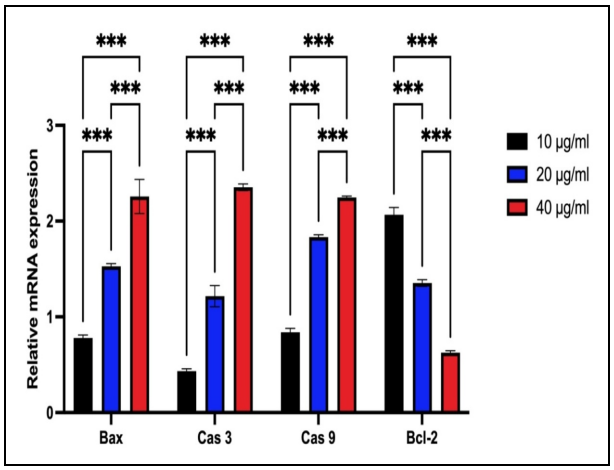

Fig. 14: Protein Expression analysis after treatment with the CB-ZnO-NPs in human lung cancer cells

3.11 Protein Expression Analysis

Apoptosis is regulated by many proteins. Figure. 14 displays the expression levels of proteins namely Bax, caspase-3, caspase-9, Bcl-2, and the internal marker b-actin, to determine the apoptotic pathway via which CB-ZnONPs induce cell death. Our findings indicate that the levels of several proteins, including Bax, caspase-3, and caspase-9, are altered in cells treated with CB-ZnONPs in a manner that is dependent on the dosage. The internal control protein actin remained constant throughout the duration of the experiment. Our findings align with the research conducted by (Ahamed *et al.* 2012; Li *et al.* 2020), which emphasized the initiation of an inherent pathway involving Caspase activation in cell death.

4. CONCLUSION

Simple hydrothermal synthesis of chavibetol coated ZnO nanoparticles was achieved. Producing highly crystalline, uniformly sized, and unloaded zinc oxide nanoparticles is made straightforward with the slightly modified hydrothermal process. ZnO nanoparticles were put into the powerful anticancer model medication chavibetol. Successful conjugation of Chavibetol on the surface of ZnO nanoparticles was verified by FT-IR analysis. We varied the pH conditions to see the regulated release pattern of chavibetol from the zinc oxide nanoparticles. The release of chavibetol was higher in acid medium. Thus, our composition can be applied as a useful drug delivery system and, at very low concentrations, because of a notable lethal effect in the chosen lung cancer cells. Moreover, it was demonstrated to be able to cause apoptotic processes in the chosen cancer cells. The cell death was induced through an inherent apoptosis pathway inferred through western blot analysis. Our produced nanoparticles, taken together, considerably reduce the in vitro development of lung cancer cells. Optimization of the produced nanoparticles as a candidate for evaluation in animal models should require more research.

FUNDING

This research received no specific grant from any funding agency in the public, commercial, or not-for-profit sectors.

CONFLICTS OF INTEREST

The authors declare that there is no conflict of interest.

REFERENCES

Aara, A., Chappidi, V. and Ramadas, M., Antioxidant activity of eugenol in Piper betel leaf extract, *J. Fam. Med. Prim. Care*, 9(1), 327 (2020). https://doi.org/10.4103/jfmpc.jfmpc_809_19

Abayarathne, H. M. I., Dunuweera, S. P. and Rajapakse, R. M. G., Synthesis of cisplatin encapsulated Zinc oxide nanoparticles and their application as a carrier in targeted drug delivery, *Ceylon J. Sci.*, 49(1), 71 (2020). https://doi.org/10.4038/cjs.v49i1.7707

Ahamed, M., Javed Akhtar, Kumar, Khan, M. and Ahmad, Alrokayan, Zinc oxide nanoparticles selectively induce apoptosis in human cancer cells through reactive oxygen species, *Int. J. Nanomed.*, 845 (2012). https://doi.org/10.2147/IJN.S29129

Aljabali, A. A. A., Obeid, M. A., Bakshi, H. A., Alshaer, W., Ennab, R. M., Al-Trad, B., Al Khateeb, W., Al-Batayneh, K. M., Al-Kadash, A., Alsotari, S., Nsairat, H. and Tambuwala, M. M., Synthesis, Characterization, and Assessment of Anti-Cancer Potential of ZnO Nanoparticles in an In Vitro Model of Breast Cancer, *Molecules*, 27(6), 1827 (2022). https://doi.org/10.3390/molecules27061827

Alrushaid, N., Khan, F. A., Al-Suhaimi, E. A. and Elaissari, A., Nanotechnology in Cancer Diagnosis and Treatment, *Pharmaceutics*, 15(3), 1025 (2023). https://doi.org/10.3390/pharmaceutics15031025

Anjum, S., Hashim, M., Malik, S. A., Khan, M., Lorenzo, J. M., Abbasi, B. H. and Hano, C., Recent Advances in Zinc Oxide Nanoparticles (ZnO NPs) for Cancer Diagnosis, Target Drug Delivery, and Treatment, *Cancers (Basel)*, 13(18), 4570 (2021). https://doi.org/10.3390/cancers13184570

Asif, N., Amir, M. and Fatma, T., Recent advances in the synthesis, characterization and biomedical applications of zinc oxide nanoparticles, *Bioprocess Biosyst. Eng.*, 46(10), 1377–1398 (2023). https://doi.org/10.1007/s00449-023-02886-1

Baranwal, J., Barse, B., Di Petrillo, A., Gatto, G., Pilia, L. and Kumar, A., Nanoparticles in Cancer Diagnosis and Treatment, *Materials (Basel)*, 16(15), 5354 (2023). https://doi.org/10.3390/ma16155354

Halanayake, K. D., Kalutharage, N. K. and Hewage, J. W., Microencapsulation of biosynthesized zinc oxide nanoparticles (ZnO-NPs) using Plumeria leaf extract and kinetic studies in the release of ZnO-NPs from microcapsules, *SN Appl. Sci.*, 3(1), 17 (2021). https://doi.org/10.1007/s42452-020-04100-3

Jin, S. E. and Jin, H. E., Synthesis, Characterization, and Three-Dimensional Structure Generation of Zinc Oxide-Based Nanomedicine for Biomedical Applications, *Pharmaceutics.*, 11(11), 575 (2019). https://doi.org/10.3390/pharmaceutics11110575

Kulothungan, V., Sathishkumar, K., Leburu, S., Ramamoorthy, T., Stephen, S., Basavarajappa, D., Tomy, N., Mohan, R., Menon, G. R. and Mathur, P., Burden of cancers in India - estimates of cancer crude incidence, YLLs, YLDs and DALYs for 2021 and 2025 based on National Cancer Registry Program, *BMC Cancer*, 22(1), 527 (2022). https://doi.org/10.1186/s12885-022-09578-1

Li, J., He, J., Huang, Y., Li, D. and Chen, X., Improving surface and mechanical properties of alginate films by using ethanol as a co-solvent during external gelation, *Carbohydr. Polym.*, 123, 208–216 (2015). https://doi.org/10.1016/j.carbpol.2015.01.040

Li, Z., Guo, D., Yin, X., Ding, S., Shen, M., Zhang, R., Wang, Y. and Xu, R., Zinc oxide nanoparticles induce human multiple myeloma cell death via reactive oxygen species and Cyt-C/Apaf-1/Caspase-9/Caspase-3 signaling pathway in vitro, *Biomed. Pharmacother*, 122, 109712 (2020). https://doi.org/10.1016/j.biopha.2019.109712

Martínez, C. M., Gun'ko, Y. and Vallet-Regí, M., ZnO Nanostructures for Drug Delivery and Theranostic Applications, *Nanomaterials*, 8(4), 268 (2018). https://doi.org/10.3390/nano8040268

Nishida, N., Yano, H., Nishida, T., Kamura, T. and Kojiro, M., Angiogenesis in cancer, *Vasc. Health Risk Manag.*, 2(3), 213–219 (2006). https://doi.org/10.2147/vhrm.2006.2.3.213

Pang, R. W. and Poon, R. T., Clinical implications of angiogenesis in cancers, *Vasc. Health Risk Manag.*, 2(2), 97–108 (2006). https://doi.org/10.2147/vhrm.2006.2.2.97

Saddik, M. S., Elsayed, M. M. A., El-Mokhtar, M. A., Sedky, H., Abdel-Aleem, J. A., Abu-Dief, A. M., Al-Hakkani, M. F., Hussein, H. L., Al-Shelkamy, S. A., Meligy, F. Y., Khames, A. and Abou-Taleb, H. A., Tailoring of Novel Azithromycin-Loaded Zinc Oxide Nanoparticles for Wound Healing, *Pharmaceutics*, 14(1), 111 (2022). https://doi.org/10.3390/pharmaceutics14010111

Shah, S. C., Kayamba, V., Peek, R. M. and Heimburger, D., Cancer Control in Low- and Middle-Income Countries: Is It Time to Consider Screening?, *J. Glob. Oncol.*, (5), 1–8 (2019). https://doi.org/10.1200/JGO.18.00200

Siddiqi, K. S., ur-Rahman, A. and Tajuddin, H. A., Properties of Zinc Oxide Nanoparticles and Their Activity Against Microbes, *Nanoscale Res. Lett.*, 13(1), 141 (2018). https://doi.org/10.1186/s11671-018-2532-3

Tran, K. A., Kondrashova, O., Bradley, A., Williams, E. D., Pearson, J. V. and Waddell, N., Deep learning in cancer diagnosis, prognosis and treatment selection, *Genome Med.*, 13(1), 152 (2021). https://doi.org/10.1186/s13073-021-00968-x

Vimala, K., Sundarraj, S., Paulpandi, M., Vengatesan, S. and Kannan, S., Green synthesized doxorubicin loaded zinc oxide nanoparticles regulates the Bax and Bcl-2 expression in breast and colon carcinoma, *Process Biochem.*, 49(1), 160–172 (2014). https://doi.org/10.1016/j.procbio.2013.10.007